Politecnico di Milano

Facoltà di Ingegneria dei Processi Industriali

Degree in Materials Engineering and Nanotechnology

Atomic Layer Deposition of Ferroelectric Complex Oxide Thin Films

Advisor Dr. Jonathan E. Spanier

Drexel University, Philadelphia, Pennsylvania, United States of America

Co-Advisor Dr. Carlo S. Casari

Politecnico di Milano, Milano, Italia

Co-Advisor Dr. Spain Advisor

Universidad Politécnica de Madrid, Madrid, España

Master's Thesis Presented by:

Brian R. Beatty

Matricola: 780703

Academic Year 2011-2012

For my parents...

Contents

List of Figures

List of reactions

Acknowledgements

First and foremost, I would like to acknowledge all of the support that my advisor, Dr. Jonathan Spanier, gave me at Drexel.

Eric Gallo, Maria Sancho-Torres, Stephen Nonenmann, Stephanie Johnson

Keith Fahnestock

Other Professors in MATE dept.

Abstract

Blah blah blah ferroelectric stuff.

As devices based on ferroelectric films become more commonplace, a commercially viable process for fabricating the material is needed; low cost and high volume are implied necessities for such a process. This work focuses on the application of atomic layer deposition (ALD) to this task. ALD is a standard fabrication process in the electronics industry, valuable for its high uniformity across large surfaces, capability to control film thickness with very high resolution, and conformality across three dimensional structures. The various tasks in designing and optimizing an ALD process, as well as characterization methods for analysis of the produced films, will be discussed in detail.

Work supported by ARO? under Grant #.

Sommario

this part has to be a detailed description of the project written completely in italian. sad face.

Chapter 1

Introduction

1.1 Scope of this work

Chapter 2

Lead Titanate

2.1 Structure

Lead titanate ($PbTiO_3$, PTO) naturally orders into the tetragonal perovskite crystal structure at room temperature (figure 2.1). The structure can be affected by compositional changes, temperature, or strain (primarily in thin-film systems), allowing a transition to a cubic phase. In the perovskite crystal structure, the central cation (Ti^{4+} in the case of $PbTiO_3$) is encapsulated in a octahedral cage of anions (O^{2-}), with the remaining cations (Pb^{2+}) situated in the eight corners of the unit cell. if the material was doped (as in a mixed solid-solution), some of the cations would be replaced with the dopant ions, for example Zr^{4+} would be randomly distributed in Ti^{4+} sites in the $PbTi_{1-x}Zr_xO_3$ (PZT) system.

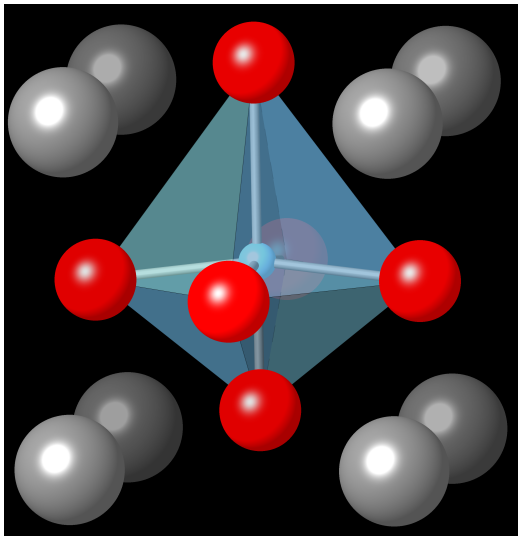

Figure 2.1: Tetragonal perovskite structure of $PbTiO_3$.
Grey, red, or blue spheres refer to Pb^{2+}, Ti^{4+}, or O^{2-}, respectively

2.1.1 Effect of Temperature

The transition from tetragonal to cubic perovskite is highly dependent on temperature. The critical temperature at which this transition occurs is referred to as the Curie temperature (T_C). If the material cools through this temperature, a lengthening of the 'c' axis of the unit cell spontaneously occurs. This creates anisotropy in the structure and allows for an anisotropic charge distribution to develop. In lead titanate this is caused by the shifting of the titanium ion, along with a slight shift of some of the oxygen ions as well

(visible in figure 2.1). Thus, a permanent dipole is created whose magnitude increases as the system cools further from T_C. This permanent dipole allows the system to exhibit ferroelectricity, implying an ability to semi-permanently switch the orientation of the dipole in the material. This switching can be reversed, but this will not occur spontaneously.

2.2 Ferroelectricity

Chapter 3

Synthesis Methods

Synthesis of perovskite oxides has been demonstrated using a wide range of techniques. These range from solution-based processing methods (sol-gel approach), to physical vapor methods (molecular beam epitaxy and pulsed laser deposition), and gas phase chemical methods (chemical vapor deposition and atomic layer deposition). This review will briefly discuss sol-gel, physical vapor deposition, as well as CVD methodology, but will focus in more depth on films deposited via ALD.

3.1 Sol-Gel Processing

3.2 Physical Vapor Deposition

3.3 Metallorganic Chemical Vapor Deposition

3.4 Atomic Layer Deposition

Atomic Layer Deposition (ALD) is a modification on standard CVD processes, with a few major differences. The defining aspect of an ALD process is the separation of the overall reaction into two steps: first the precursor is allowed to react with the substrate surface (see reaction 3.1), excess reactant is purged from the chamber and an oxidizer is introduced to complete the reaction (see reaction 3.2). These reactions show a very simple ALD reaction between trimethylaluminum (TMA) and water.

$$\mathrm{Al(CH_3)_3 + M{-}OH_{surf} \longrightarrow M{-}O{-}Al(CH_3)_{2\,surf} + CH_4} \quad \{3.1\}$$

$$\mathrm{M{-}O{-}Al(CH_3)_{2\,surf} + 2\,H_2O \longrightarrow M{-}O{-}Al(OH)_{2\,surf} + 2\,CH_4} \quad \{3.2\}$$

In this example, it is seen that the first stage allows the TMA to react with the hydrated substrate surface to form part of a layer of alumina (Al_2O_3), liberating a molecule of methane as a byproduct. In the next step, the remaining ligands are stripped away from the bound TMA molecule and replacing them with hydroxy groups. This returns the system to the initial state — where the surface is presenting sites available to react with more TMA — and the cycle is completed.

Having only surface reactions be permitted, as opposed to CVD where gas-phase interactions dominate, affords ALD a number of unique characteristics. One of these is the concept of the "self-limiting" growth mode. This behavior arises from the limited

number of available reaction sites; when all of these have either been reacted with or made unavailable by a blocking mechanism such as stearic hindrance from other local chemisorbed precursor the reaction can no longer proceed. At this point, additional available precursor is not going to be utilized, and instead will be removed and treated as waste material. The system is then evacuated, and a inert purge gas such as dry nitrogen or argon (at UHP grade) is flowed through the reactor. The purge gas serves both to push any remaining gases out of the reactor as well as to help desorb physisorbed species from the surface. If these are allowed to remain adsorbed they would react with the oxidant and negate the surface-limited aspects of ALD. The system would then again be evacuated, and the oxidant introduced and then pumped away to complete the cycle.

In the implementation of most ALD systems, the purge gas is also used as a carrier gas for the precursors. Thus a constant flow of gas is passed through the system, instead of having it occasionally fully evacuated, and the precursor is able to be delivered from its source to the reactor more effectively. For some precursor compounds, in particular those with a low vapor pressure, having carrier-assisted transportation can greatly improve the behavior of the system.

Because of the self-limiting behavior, each deposition cycle is limited to a theoretical maximum of one monolayer of material (in practice a much lower coverage per cycle is attained), which is far less than a unit cell. Generally per cycle growth rates range between 0.03–1.5Å, with the rate being nearly invariable during most of the deposition. This gives the second defining characteristic of ALD: very high (Å level) thickness resolution. The downside of this aspect is that growths are generally much slower than other types of depositions; ALD is generally slower by an order of magnitude or more than a similar CVD process, as an example. This has proved invaluable in many processes where high precision is critical, such as electronics manufacturing. Intel, for example, uses ALD to deposit extremely thin layers of a high-κ dielectric (such as hafnia, HfO_2) for use as the gate oxide in its transistors, with layer thickness generally less than 2nm.

This method will produce a layer of a binary oxide material (AO_x), if more complex materials are desired the method must be changed. The basic principles remain the same; one would perform the procedure for depositing a cycle of a binary oxide and then change the precursor and deposit another cycle of a different oxide material. For example, if one wished to deposit $PbTiO_3$, one would begin by depositing a layer of TiO_2 and then depositing a layer of lead oxide (PbO). Repeating this set of cycles — a super-cycle — would eventually form the $PbTiO_3$ film.

However, deposition of complex oxides is not this simple in practice. In many cases, running each oxide cycle in a 1:1 ratio will deposit a non-stoichiometric material. This makes it necessary to modify the method to deposit more of one type of oxide than the other. For example, if a material is Ti-rich the super-cycle ratio would be modified to increase the number of lead oxide cycles as compared to the titania cycles. Needs more here.

ALD reactions are rather sensitive to a number of factors, such as temperature. The temperature must be high enough that the reactants have sufficient energy to drive the surface reaction but not so high as to allow undesirable reactions to activate (e.g. precursor cracking or surface material desorption). Precursor selection is also very important, for similar reasons. The precursors must also be incapable of reacting with themselves, to allow the self-limiting mechanism to work properly. This section needs more work.

Chapter 4

Characterization Methods

4.1 Imaging Techniques

A variety of imaging methods were used to visually inspect the samples at a variety of length scales. The two main techniques that proved invaluable for this aspect of the project were scanning electron microscopy (SEM) as well as atomic force microscopy (AFM).

4.1.1 Scanning Electron Microscopy

Scanning electron microscopy is a widely used technique for imaging nanostructures.

4.1.2 Atomic Force Microscopy

4.2 Compositional Analysis

4.2.1 Energy-Dispersive X-Ray Spectroscopy

4.2.2 X-Ray Fluorescence Spectroscopy

4.2.3 Rutherford Backscattering Spectroscopy

4.3 Thin Film Characterization

4.3.1 Variable Angle Spectroscopic Ellipsometry

Ellipsometry is a powerful non-destructive optical technique that allows for the determination of a large number of properties of complex thin film structures. The basic tenet of ellipsometry relies on the analysis of the change in polarization state of a reflected light beam after interaction with the sample. The incident beam is generally linearly polarized, but upon reflection becomes elliptically polarized due to a phase shift in the components of the beam in the s- and p-plane, as well as a change in their relative amplitudes. The phase shift is correlated to the ellipsometric parameter Δ, while the amplitude change is given by $\tan\Psi$ (Ψ is the angle between the s-plane and the major axis of the ellipse). The last major parameter is the incident angle, denoted by ϕ. A schematic diagram illustrating these parameters can be seen in figure 4.1.

From these parameters, one can directly determine the ratio between the reflectance in the p-plane (r_p) and the reflectance in the s-plane (r_s) from the fundamental ellipsometric relation (eqn. 4.1). Once this relationship is known, the Fresnel equations (eqn. 4.2) can be

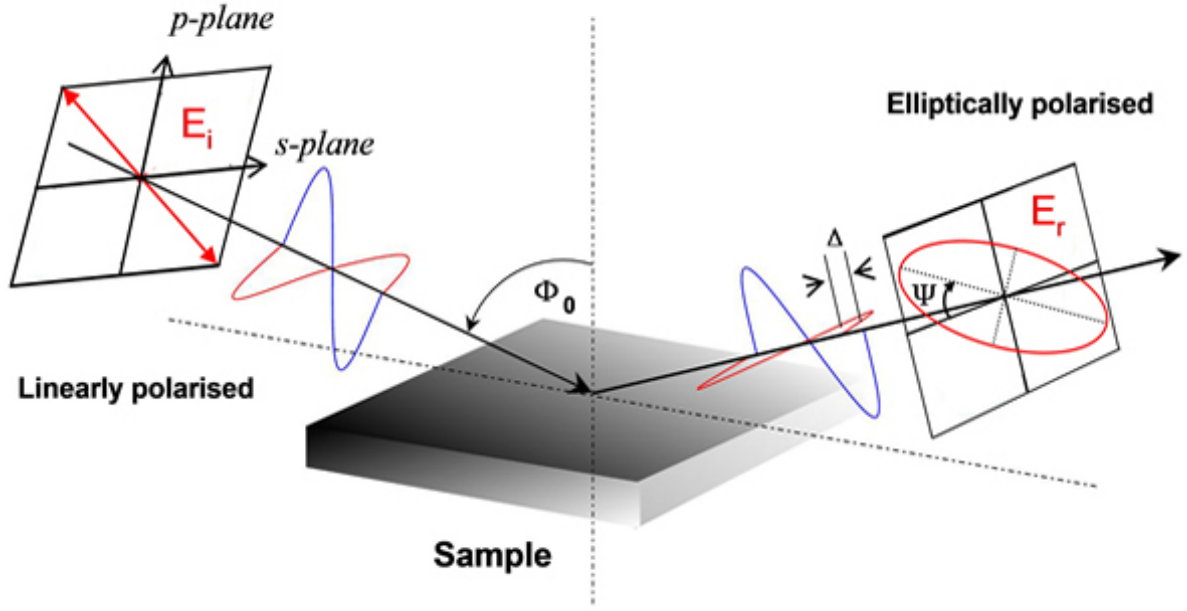

Figure 4.1: Schematic of the beam path during an ellipsometric measurement, critical parameters are indicated

used to numerically determine the value of the complex index of refraction at the specific wavelength of the incoming beam. The complex index of refraction (eqn. 4.3) describes the nominal index of refraction but additionally includes an imaginary term to describe absorption of light in the material (commonly referred to as the extinction coefficient, κ).

$$\rho = \frac{r_p}{r_s} = \tan(\psi)e^{i\Delta} \tag{4.1}$$

$$r_p = \frac{\tilde{n}_1\sqrt{1-\left(\frac{\tilde{n}_1}{\tilde{n}_2}\sin\phi\right)} - \tilde{n}_2\cos\phi}{\tilde{n}_1\sqrt{1-\left(\frac{\tilde{n}_1}{\tilde{n}_2}\sin\phi\right)} + \tilde{n}_2\cos\phi} \tag{4.2a}$$

$$r_s = \frac{\tilde{n}_1\cos\phi - \tilde{n}_2\sqrt{1-\left(\frac{\tilde{n}_1}{n_2}\sin\phi\right)}}{\tilde{n}_1\cos\phi + \tilde{n}_2\sqrt{1-\left(\frac{\tilde{n}_1}{\tilde{n}_2}\sin\phi\right)}} \tag{4.2b}$$

$$\tilde{n} = n + i\kappa \tag{4.3}$$

This type of analysis is sufficient for thick, isotropic samples without any surface layers (e.g. surface oxides or adsorbed gases), and can directly provide the value of $\tilde{n}$. However, once layers are stacked upon one another, the system becomes very difficult to analyze directly due to interference effects between the layers. It becomes necessary to

use modeling techniques to determine the correct values of $\tilde{n}$ and thickness (t) for each layer.

The power of ellipsometry as a high-resolution optical analysis technique stems from the use of phase and polarization changes. This allows the analysis to overcome the diffraction limit, and can be accurate down to angstroms. Properly modeling the system is critical for this analysis to be as precise as possible. Thus, there have been refinements of the ellipsometric method to greatly increase the amount of experimental data points, allowing the overall system to be over-determined and thus letting all of the systems parameters to be calculated.

Variable angle spectroscopic ellipsometry (VASE) is one of these variants. Spectroscopic ellipsometry differs from single-wavelength ellipsometry by utilizing a broad-band light source as opposed to a monochromatic source. By performing ellipsometric analysis at each of the wavelengths, one can determine the wavelength (and thus photon-energy) dependence of n and κ. This not only helps to improve data analysis (as it can generally be safely assumed that the values of n and κ are smooth functions of λ), but allows for the determination of many other properties of the material. Of specific importance is the complex dielectric function ($\tilde{\epsilon}$), which is related to $\tilde{n}$ by the relation shown in equation 4.4. Knowing this function can allow for determination of electronic properties such as the bandgap energy, the absorption coefficient, amongst others. Finally, by obtaining spectra at a number of different incident angles, one directly provides additional data points across the entire wavelength spectrum. Even a small number of additional angles can quickly provide sufficient data points for the system to be over determined.

$$\tilde{\epsilon} = \epsilon_1 + i\epsilon_2 = \tilde{n}^2 \tag{4.4}$$

During this project, a VASE M-2000U system (figure 4.2) built by J.A. Woollam, inc. was used to collect all of the ellipsometric data. In addition, data analysis was performed using the WVASE32 package also provided by J.A. Woollam. The system utilizes a rotating compensator and a CCD detector to greatly decrease data collection time by collecting data across the entire spectrum simultaneously. More information on this system is available on J.A. Woollam, inc.'s webpage.[1]

Figure 4.2: Photograph of the J.A. Woollam M-2000U variable angle spectroscopic ellipsometer (VASE)

4.4 Phase Identification

4.4.1 X-Ray Diffraction

4.4.2 Grazing Incidence X-Ray Diffraction

4.5 Chemical Analysis

4.5.1 Thermogravimetric Analysis

4.5.2 Differential Scanning Calorimetry

Chapter 5

Sample Fabrication

5.1 Precursor Selection

5.1.1 Titanium Source

5.1.2 Lead Source

5.2 Substrate Preparation

5.2.1 Si(100)

5.2.2 Platinized Si(100)

5.2.3 STO(100) and Nb:STO(100)

5.3 Deposition Parameters

5.3.1 Growth Temperature

5.3.2 Purge Time

5.3.3 Exposure Time

5.4 Post-Deposition Annealing

Chapter 6

Data Collection and Analysis

6.1 VASE and Modeling

Ellipsometry was used extensively to determine a variety of properties of the material. However, the primary goal of ellipsometric analysis was to determine the film thickness, in order to be able to determine the film growth rate (in terms of Å per deposition cycle) of the process.

6.1.1 Data Collection

In order to collect the experimental data, the following series of steps were followed:

1. Optics alignment
2. Ambient light compensation (DC offset)
3. Data collection at multiple angles

Alignment of the optics of the system is performed in the manner described in the ellipsometer manual.[2] The system can have focusing optics installed which diminish the spot size of the analysis, which is useful if inhomogeneity is expected in the sample as this is a major problem for analysis (two of the main assumptions made by ellipsometric models are that the layers have consistent thicknesses and optical behavior across the analysis area). This is done by manually adjusting the sample stage height and the sample surface plane. The system is designed so that when the incoming signal is maximized the sample is properly aligned with respect to the p- and s-planes defined by the equipment.

Once the system is aligned, the signal that is due to ambient light (not produced by the light source) must be compensated for. The M-2000U defines this as the "DC offset."[2] The offset is calibrated automatically by the system by blocking the light source and measuring the signal from the surroundings. As the light present in the room is generally randomly polarized, the signal will be invariant to the polarizer settings. Correctly setting this value greatly decreases the uncertainty during the analysis phase; it mainly affects the degree of light depolarization measured by the system. The ellipsometer includes the depolarization in its calculation of the confidence interval for the final measurement. If the degree of ambient unpolarized light is not determined before the measurement, the depolarization will be nearly completely unrelated to the actual depolarization by the sample. In addition, the depolarization can be used by non-idealized models to determine such parameters as layer thickness variation, or internal interface roughness. This process

will not be used for the remainder of this discussion, but more information can be found in the manual for the M-2000U.[2]

After the calibration steps have been completed, data collection can be performed. Three different incident angles were used for the data collection: 55°, 60°, and 65°. At each angle, the data was averaged over three hundred revolutions of the compensator to minimize noise in the experimental data. The system was set up to collect depolarization data simultaneously with the ellipsometric parameters.[2]

If the sample is expected to be inhomogeneous, the focusing optics can be used and data collected at several different locations on the sample. This can provide data on how the growth process behaves spatially, such as if there is abnormal growth near the edges of the sample but homogeneous deposition as one moves nearer to the center of the substrate.

6.1.2 Model Definition

The definition of the model is a critical part of the analysis procedure. The model dictates how the software package will perform its various calculations to predict the overall optical behavior, which it iteratively compares to the experimentally determined ψ and Δ.

Simply put, the model is defined as a bulk (semi-infinite) substrate layer, with a nominal number of nano- to micrometer thick layers stacked upon it. Each layer is modeled with a prediction of optical constants at each test wavelength. These optical constants can be provided as a table of experimentally determined results, which are available for many commonly used materials such as silicon, silica, titania, amongst others; they can also be predicted using a variety of different models. These can be empirical predictors, such as the Cauchy dispersion, or based upon physical properties of the material, oscillator-based models for example. The model types relevant to this work are discussed in more detail in subsequent sections.

The four different substrates require different material layer stacks to properly represent them, and each poses individual challenges for characterization. The Si(100) substrate that was most commonly used for this work was the simplest to model. It can be represented as a substrate layer of silicon, with a 200nm layer of silica on top. The deposited film would be layered above the SiO_2 layer (see fig. 6.1 for a schematic representation). A large number of these substrates were analyzed for their oxide layer thickness, where the only parameter to be fit was the layer thickness. It was found that the nominal oxide layer was 200 $\pm$ 5nm thick. This was consistent enough that 200nm could be used for the initial thickness estimate for all samples using this substrate, and after the ALD layer was analyzed this thickness could also be included in the fit to confirm the true dimensions of the oxide layer. The substrate with thermally-grown oxide was preferred in comparison to silicon with only native oxide layer; this is because the thicker layer of transparent oxide helps to generate large oscillations in ψ and Δ, which assists in

the analysis (particularly the thickness, where the fringes are very closely related to this parameter).

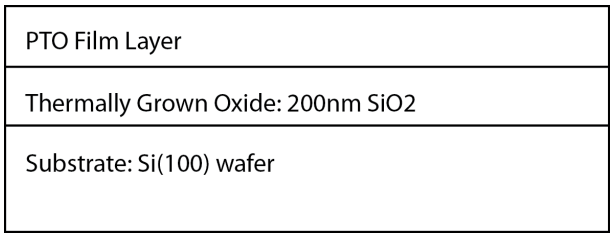

Figure 6.1: A simple graphical example of the model used for analysis of the film stack in the Si(100) samples. The unknown parameters are t and the spectroscopic values of $\tilde{n}$ for the PTO layer.

6.1.3 Analysis Procedure

Once the data was collected, a specific series of steps was followed in order to create the highest degree of accuracy from the model. All steps were performed on the PTO layer. The procedure went as follows:

1. High-λ Cauchy Model
2. Direct Calculation of n and κ
3. Conversion to Oscillator Model
4. Refinement of Oscillator Layer Parameters

This first step takes advantage of the transparency of the film at high wavelengths (low energies) where the photon energy is below the optical bandgap of the material. In this region, the Cauchy model can be used. The Cauchy model is empirical rather than physically descriptive, and best used for amorphous materials such as polymeric films, however the assumptions required for reasonable accuracy are met when absorption in the film layer is minimized (therefore $\kappa(\lambda) \approx 0$). The equations used in the Cauchy model are shown in equation 6.1. Generally, analysis during this step was performed in the spectral region where $\lambda = 600 - 1000\text{nm}$ ($E_{ph} = 2.06 - 1.24\text{eV}$).

$$n(\lambda) = A_n + \frac{B_n}{\lambda^2} + \frac{C_n}{\lambda^4} + \cdots \tag{6.1a}$$

$$\kappa(\lambda) = A_\kappa e^{B_\kappa\left(\frac{hc}{\lambda}\right) - C_\kappa} \tag{6.1b}$$

Once reasonable estimates for n, κ, and the film layer thickness are obtained at the higher wavelengths, the second step of the analysis is to generate values of $\tilde{n}$ for the rest of the spectrum. The film thickness parameter is fixed at the value determined from the Cauchy model. The values of n and κ are allowed to be determined freely without the use of a model (i.e. directly determined by use of the Fresnel relations). This type of

modeling is not physical, but assists in the generation of the oscillator-based model in the next step. The software package is then instructed to run a point-by-point fit of the data from highest- to lowest-λ, attempting to minimize the change in n or κ between adjacent data points.

This model is then inputted into a oscillator model. For the analysis of these films, a Tauc-Lorentz oscillator model was utilized. The oscillator models used by WVASE32 are expressed in terms of the complex dielectric function $\tilde{\epsilon}$, which relates to $\tilde{n}$ via the relationship in equation 6.2. The Tauc-Lorentz model changes the Lorentzian model by allowing for some absorption below the fundamental bandgap energy, which would be due to defect states and other intra-band transition mechanisms. The Tauc-Lorentz model uses the parameterization shown in equation 6.3.[2,3] ϵ_1 is provided here in a condensed version (eq. 6.3a); the full expanded version, and its derivation via Kramers-Kronig integration from ϵ_2, has been presented by Jellison and Modine.[3]

$$\tilde{\epsilon} = \epsilon_1 + i\epsilon_2 = \tilde{n}^2 \tag{6.2a}$$

$$\epsilon_1 = n^2 - \kappa^2 \tag{6.2b}$$

$$\epsilon_2 = 2n\kappa \tag{6.2c}$$

$$\epsilon_1 = \frac{2}{\pi} P \int_{E_g}^{\infty} \frac{\xi \epsilon_2(\xi)}{\xi^2 - E^2} \, \mathrm{d}\xi \tag{6.3a}$$

$$\begin{cases} \epsilon_2(E) = \dfrac{A E_0 C (E - E_g)^2}{(E^2 - E_0^2)^2 + C^2 E^2} \cdot \dfrac{1}{E} & E > E_g \quad (6.3b) \\ \epsilon_2(E) = 0 & E \leq E_g \quad (6.3c) \end{cases}$$

The WVASE32 software package allows one to use a graphical interface to provide initial guesses for the various fit parameters. At times this required multiple oscillators to best fit the predicted ϵ_2 function. Once this has been set, all of the parameters affecting ϵ_2 (A, E_0, C, E_G) are marked to be included in the fit. The software is then instructed to perform a best-fit of the oscillator to ϵ_2. Once this operation completes, the software is set to fit to ϵ_1 and only the value of the ϵ_1 offset is allowed to be fit. Finally, the software is set to optimize vs both ϵ_1 and ϵ_2, and all parameters are included. This completes the initial setup of the oscillator model.

Finally, the model is set to also allow the layer thickness to be fit and a general fit to the entire experimental dataset is performed. This provides the best guess to the physical values of the film. The thickness calculated by this procedure matches very closely to measurements performed by other methods (e.g. SEM imaging or AFM measurement of a lithographically created step). The bandgap parameter also matches well to literature values (when using standard samples of well defined materials, such as a thin layer of titania).

If similar deposition parameters are utilized, it is possible to save the parameterized model for later use. This allows the analysis to be streamlined when the material is expected to remain constant, for example if tests of deposition at different layer thicknesses are performed. In this case, the material would have optical behavior very similar to the initial sample, and the oscillator model would be sufficiently close to valid parameters to be used directly for fits. All that would need to be adjusted initially would be the estimated layer thickness. If the fit fails to produce useful data, such as unreasonable values for any of the parameters or very large confidence intervals, it is recommended to proceed with the entire standard analysis procedure.

Experimental data sets and the resulting fitted model for selected samples are presented in appendix A.5.

6.2 Composition Analysis

In order for the desired phase to be preferred, without any impurity phases precipitating, it is important to be able to control the stoichiometry of the produced film. Previous reports have shown that there is a close relationship between the composition of the film and the final resultant phase (see figure 6.2).

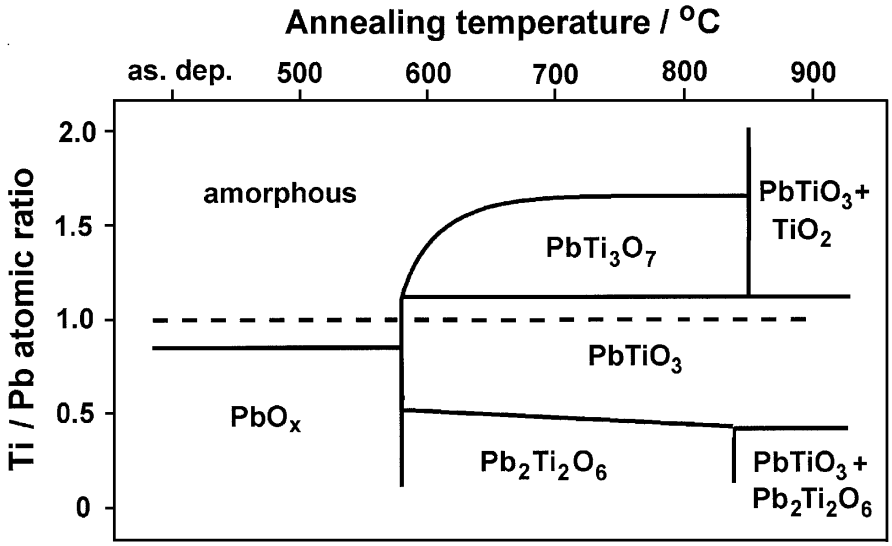

Figure 6.2: Graphic illustrating preferred phase of an annealed film at a range of stoichiometric ratios and annealing temperatures. A slight excess of Pb in the system helps to stabilize the perovskite $PbTiO_3$ phase.[4]

6.2.1 Energy-Dispersive X-Ray Spectroscopy

6.2.2 X-Ray Fluorescence Spectroscopy

6.3 X-Ray Diffraction

6.3.1 Grazing Incidence XRD

Chapter 7

Results

7.1 Ellipsometry

7.2 XRD

Chapter 8

Conclusions

8.1 Future Work

Optimize consistency

Doped materials

Other material systems (BFO, BST, etc.)

Bibliography

[1] J. A. Woollam Co., Inc. M-2000 ellipsometer. http://www.jawoollam.com/m2000_home.html.

[2] J. A. Woollam Co., Inc. *Guide to Using WVASE32*, 2009.

[3] Jr. G. E. Jellison and F. A. Modine. Parameterization of the optical functions of amorphous materials in the interband region. *Applied Physics Letters*, 69(3):371–373, 1996.

[4] J Harjuoja, A Kosola, M Putkonen, and L Niinisto. Atomic layer deposition and post-deposition annealing of PbTiO thin films. *Thin Solid Films*, 496(2):346–352, February 2006.

Appendix A

Supplemental Information

A.1 List of Samples

A.2 ALD Reactor Diagram

A.3 Recipes for S100 ALD System

A.4 Thermal Analysis Results

A.5 Ellipsometry Results

A.6 XRD Results